Behaviour of relativistic black hole accretion sufficiently close to the horizon

Paramita Barai[1], Ipsita Chakraborty[2], Tapas K Das[3,4], Paul J. Wiita[5,6]

[1] *Department de physique, Universite Laval, Quebec City, Canada,* paramita.barai.1@ulaval.ca
[2] *Adamas Institute of Technology, Kolkata 700126, India,* ipsita14@gmail.com
[3] *Harish Chandra Research Institute, Allahabad 211019, India,* tapas@hri.res.in
[4] *Theoretical Institute for Advanced Research in Astrophysics, Taiwan* tapas@tiara.sinica.tw.edu
[5] *Institute for Advanced Study, Princeton University, USA* wiita@sns.ias.edu
[6] *Department of Physics and Astronomy, Georgia State University, USA* wiita@chara.gsu.edu

Abstract

This work introduces a novel formalism to investigate the role of the spin of astrophysical black holes in determining the behaviour of matter falling onto such accretors. Equations describing the general relativistic hydrodynamic accretion flow in the Kerr metric are formulated, and stationary solutions for such flow equations are provided. The accreting matter may become multi-transonic, allowing a stationary shock to form for certain initial boundary conditions. Such a shock determines the disc geometry and can drive strong outflows. The properties of matter extremely close to the event horizon are studied as a function of the Kerr parameter, leading to the possibility of detecting a new spectral signature of black hole spin.

1 Flow Structure

The energy momentum tensor $\Im^{\mu\nu}$ has been formulated (the general most form of $\Im^{\mu\nu}$ is available in Novikov & Thorne 1973) in the Boyer-Lindquist co-ordinates, and its covariant derivative has been evaluated to obtain the general relativistic Euler equation and the equation of continuity, in the form of a set of spatio-temporal first order differential equations. Axi-symmetry has been adopted for the flow geometry as described in figure 1, where, following Abramowicz, Lanza & Percival (1997), the disk height $h(r)$ is calculated as:

$$h(r) = \sqrt{\frac{2}{\gamma+1}} r^2 \left[\frac{(\gamma-1)c_c^2}{\{\gamma-(1+c_s^2)\}\{\lambda^2 v_t^2 - a^2(v_t-1)\}}\right]^{\frac{1}{2}} \tag{1}$$

Two first integrals of motion for the system defined along streamlines, the conserved specific flow energy, $\mathcal{E}$ and the baryonic load rate, $\dot{M}$, along with the corresponding entropy accretion rate, $\dot{\Xi}$, are calculated as:

$$\mathcal{E} = \left[\frac{(\gamma-1)}{\gamma-(1+c_s^2)}\right]\sqrt{\left(\frac{1}{1-u^2}\right)\left[\frac{Ar^2\Delta}{A^2-4\lambda arA+\lambda^2 r^2(4a^2-r^2\Delta)}\right]}\,, \quad \dot{M} = 4\pi\Delta^{\frac{1}{2}} H\rho\frac{u}{\sqrt{1-u^2}}\,, \tag{2}$$

$$\dot{\Xi} = \left(\frac{1}{\gamma}\right)^{\left(\frac{1}{\gamma-1}\right)} 4\pi\Delta^{\frac{1}{2}} c_s^{\left(\frac{2}{\gamma-1}\right)} \frac{u}{\sqrt{1-u^2}}\left[\frac{(\gamma-1)}{\gamma-(1+c_s^2)}\right]^{\left(\frac{1}{\gamma-1}\right)} H(r) \tag{3}$$

Differential solutions of the first integrals of motion provides the three velocity gradient (of the flow) as a first order autonomous dynamical system:

$$\frac{du}{dr} = \frac{\frac{2c_s^2}{(\gamma+1)}\left[\frac{r-1}{\Delta}+\frac{2}{r}-\frac{v_t\sigma\chi}{4\psi}\right]-\frac{\chi}{2}}{\frac{u}{(1-u^2)}-\frac{2c_s^2}{(\gamma+1)(1-u^2)u}\left[1-\frac{u^2 v_t\sigma}{2\psi}\right]}, \tag{4}$$

In Eqns. (1–4), $r, u, c_s, \rho, \lambda, \gamma, a$ are the radial distance on the equatorial plane, three (flow) velocity, sound speed, density, flow specific angular momentum, flow adiabatic index and the black hole spin (the Kerr parameter) respectively. A and Δ are functions of r and a, v_t is function of $u, r, \lambda, a, A, \Delta$, and other terms (especially in (4)) are functions of above quantities and of various metric elements as well as their space derivatives. Further details about the above mentioned equations are available in Barai, Das & Wiita (2004).

2 Transonicity, Shock and Outflow Generation

The fixed point solution obtained from (4) provides the number of critical points the flow can pass through, and thus provides the number of transonic flips.

Region of multi-transonicity for both accretion (marked A) and wind (marked W) in the parameter space are shown in figure 2. The labels I and O indicate regions with lone inner and outer critical points, respectively. The plot has been generated for $a = 0.3$ and $\gamma = 1.33$.

Multi-transonic (actually, bi-modal, since the middle sonic point does not support a steady solution that passes through it) accretion flows may encounter a stationary shock. The general relativistic shock conditions are formulated:

$$[[\rho u \Gamma_u]] = 0, [[\Im_{t\mu}\eta^\mu]] = [[(p+\epsilon)v_t u\Gamma_u]] = 0, [[\Im_{\mu\nu}\eta^\mu\eta^\nu]] = \left[\left[(p+\epsilon)u^2\Gamma_u^2 + p\right]\right] = 0, \tag{5}$$

where Γ_u is the Lorentz factor, and η_μ is the normal to the hypersurface Σ of discontinuity. The expression for the shock invariant $\mathcal{S}_h$ is computed:

$$\mathcal{S}_h = c_s^{\frac{2\gamma+3}{\gamma-1}} \left(\gamma - 1 - c_s^2\right)^{\frac{3\gamma+1}{2(1-\gamma)}} u \left(1-u^2\right)^{-\frac{1}{2}} \left[\lambda^2 v_t^2 - a^2\left(v_t - 1\right)\right]^{-\frac{1}{2}} \left[\frac{u^2\left(\gamma - c_s^2\right) + c_s^2}{c_s^2\left(1-u^2\right)}\right] \tag{6}$$

The shock strength and the entropy enhancement ratio (at the shock) are defined as the ratios of Mach numbers (M_-/M_+) and the entropy accretion rate (Ξ_+/Ξ_-) respectively, where $-$ and $+$ indicate the pre- and post-shock values of any flow variable.

Simultaneous solution of Eqns. (1–6) provides the phase portrait of the shocked multi-transonic accretion, as shown in figure 3. Transonic flow (marked by 'A') through the outer sonic point encounters a stable stationary Rankine-Hugoniot shock transition marked by S1 (S2 being the other formal shock location, which is unstable and hence is not considered), produces post shock subsonic flow, which again becomes supersonic (segment marked by 'a') after passing through the inner sonic point; and finally plunges through the event horizon. As a consequence of the shock formation, the post shock flow has higher temperature, density, pressure and residence time compared to its pre-shock counterpart. This favours the generation of an optically thick halo (yellow coloured elliptic patches in figure 4, where the disc structure has been obtained by solving (1-6)) in the post shock region as a result of disc evaporation, and initiates the production of thermally and centrifugally driven cosmic outflows.

Figure 5a shows the variation of shock location r_{sh} as a function of black hole spin. Figure 5b shows that the stronger shocks (higher value of (M_-/M_+)) are produced closer to the black hole, and is a result of maximum entropy production (measured by (Ξ_+/Ξ_-)) due to the shock. Pre- and post-shock ratios of temperature, pressure, density and velocity (some of the normalized by appropriate numerical factors so as to fit in the same figure) as a function of black hole spin are plotted in figure 5c.

3 Quasi-terminal Values

Flow variables (calculated along the solution 'a') at a very close proximity $r_\delta = r_+ + \delta$ ($r_+ = 1 + \sqrt{(1-a^2)}$, and $\delta = 0.001 r_g$) of the event horizon are termed as quasi-terminal values, and are

distinguished with a subscript δ. The variation of the (normalized) quasi-terminal temperature (T_δ), density (ρ_δ), pressure (p_δ), as a function of the black hole spin, are shown in the figure 6. The calculations are performed for a $3\times10^6 M_\odot$ black hole accreting at a rate of $4.29\times10^{-6} M_\odot \mathrm{Yr}^{-1}$.

Shock formation is naturally also possible for other values of the black hole mass and the accretion rate, as well as for values of the black hole spin higher than those shown here in Fig. 6. Accretion onto the rotating black hole with the Kerr parameter as high as 0.95 has been observed to form shocks; the details of such work will be reported elsewhere (Barai, Chakraborty, Das & Wiita, in preparation).

4 Conclusion

- For the first time, the shocked relativistic accretion in the Kerr metric has been studied at such a close proximity to the black hole event horizon.
- The effects of the black hole spin on the dynamical and thermodynamical properties of the accreting material have been made explicit.
- Accurate estimates of the flow temperature, velocity and density profile has been made. This leads to a possible formalism for the study of the spectral signature of the black hole spin (work in progress).

Acknowledgements

The work of TKD was partially supported by the Theoretical Institute for Advanced Research in Astrophysics (TIARA) operated under Academia Sinica and the National Science Council Excellence Projects program in Taiwan, administered through grant NSC 96-2752-M-007-007-PAE. IC would like to acknowledge the kind hospitality provided by HRI, Allahabad, India.

References

[1] Abramowicz, M. A., Lanza, A., & Percival, M. J. 1997, ApJ, 479, 179.

[2] Barai P, Das T K, Witta P J, 2004, Astrophys. J. Lett., 613, L49.

[3] Novikov, I., & Thorne, K. S., 1973, in Black Holes. ed. DeWitt, C. & DeWitt, B. Gordon & Breach. NY. p. 343.

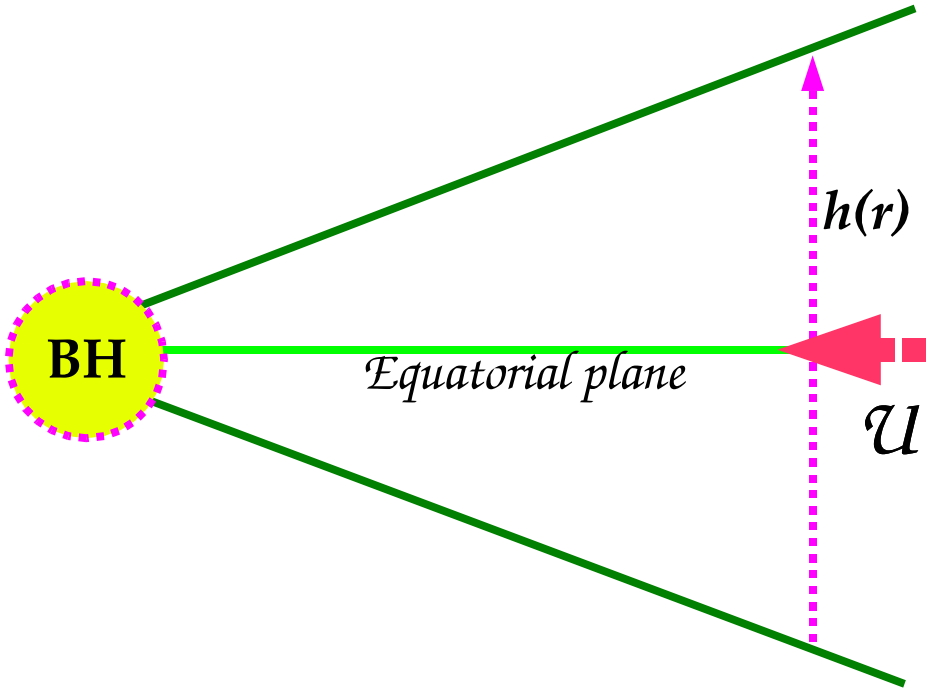

Figure 1: The yellow circular patch with BH written inside represents the black hole and the pink dashed boundary mimics the event horizon. The wedge shaped dark green lines represents the envelop of the accretion disc. The light green line centrally flanked by the two dark green disk boundaries, is the equatorial plane, on which all of the dynamical quantities (e.g., the advective three velocity u) are assumed to be confined. Any thermodynamic quantity (e.g., the flow density) is averaged over the local disc height $\mathbf{h}(r)$.

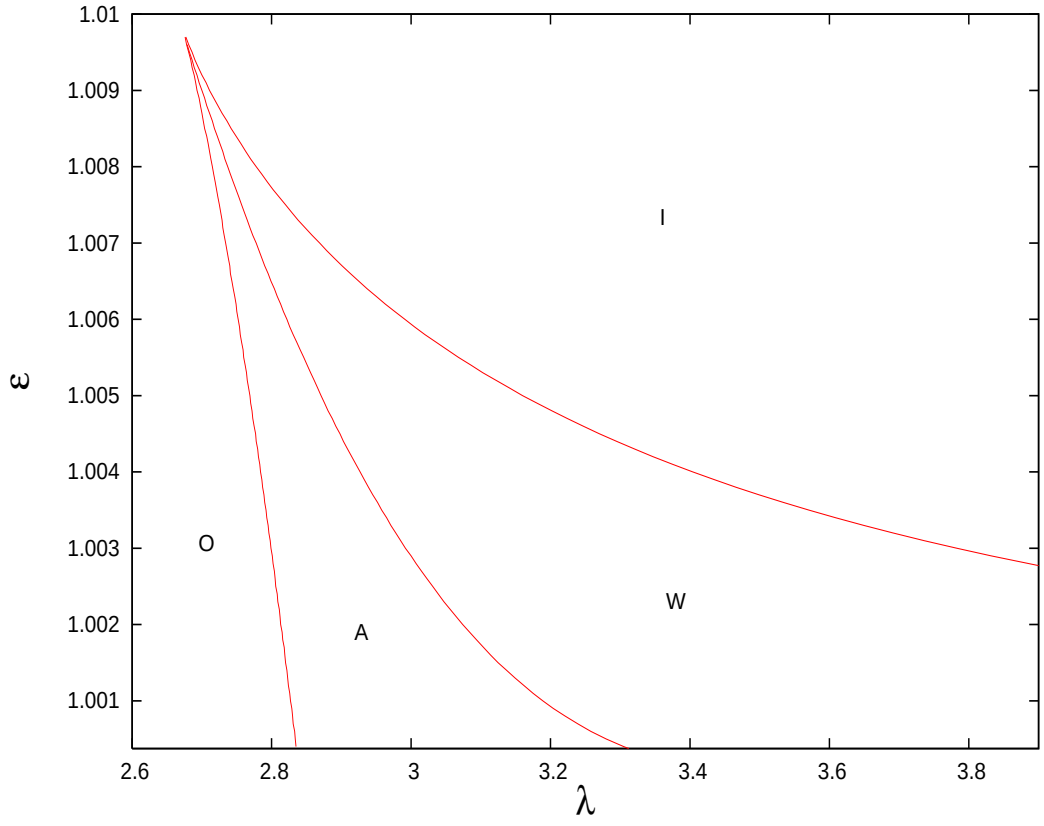

Figure 2

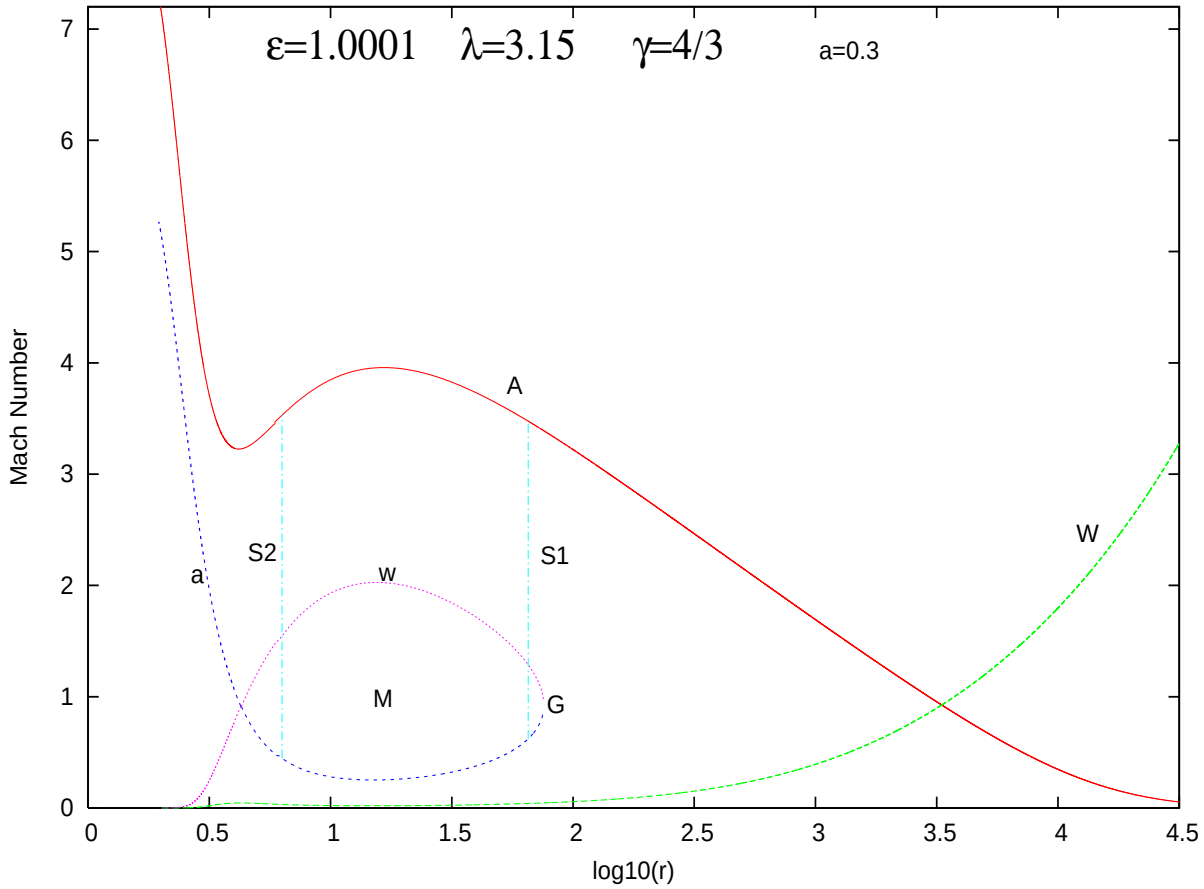

Figure 3

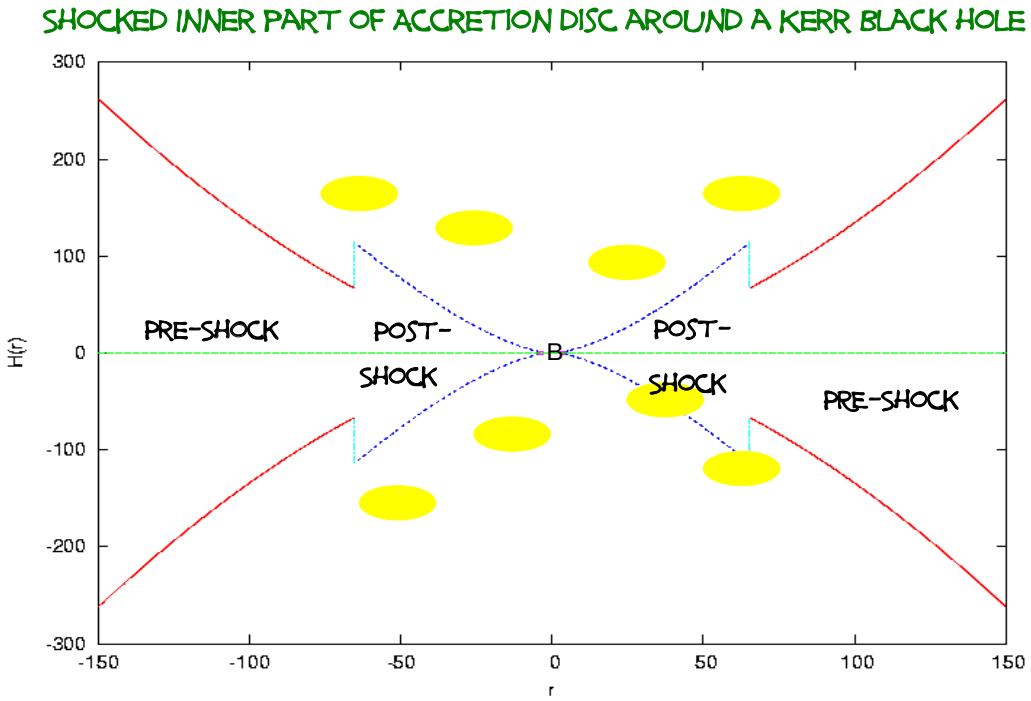

Figure 4: Pre- and post-shock disc geometry with thermally driven optically thick halo.

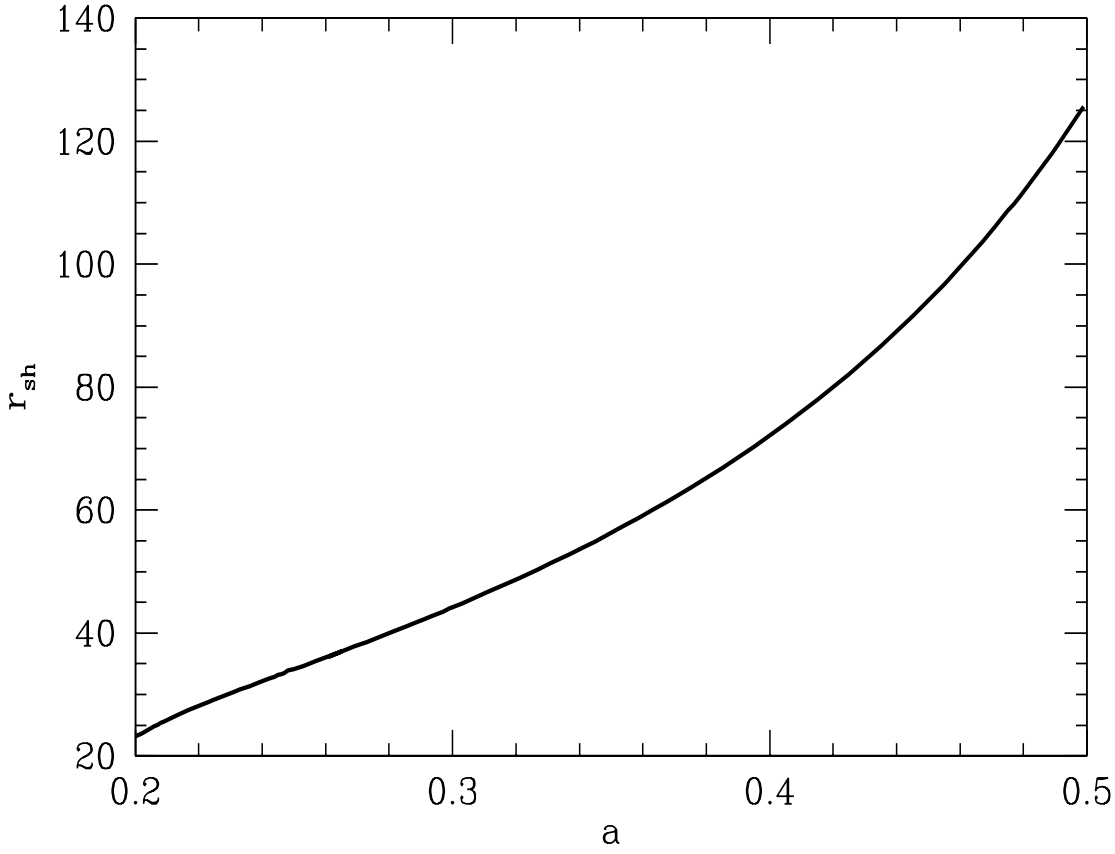

Figure 5a

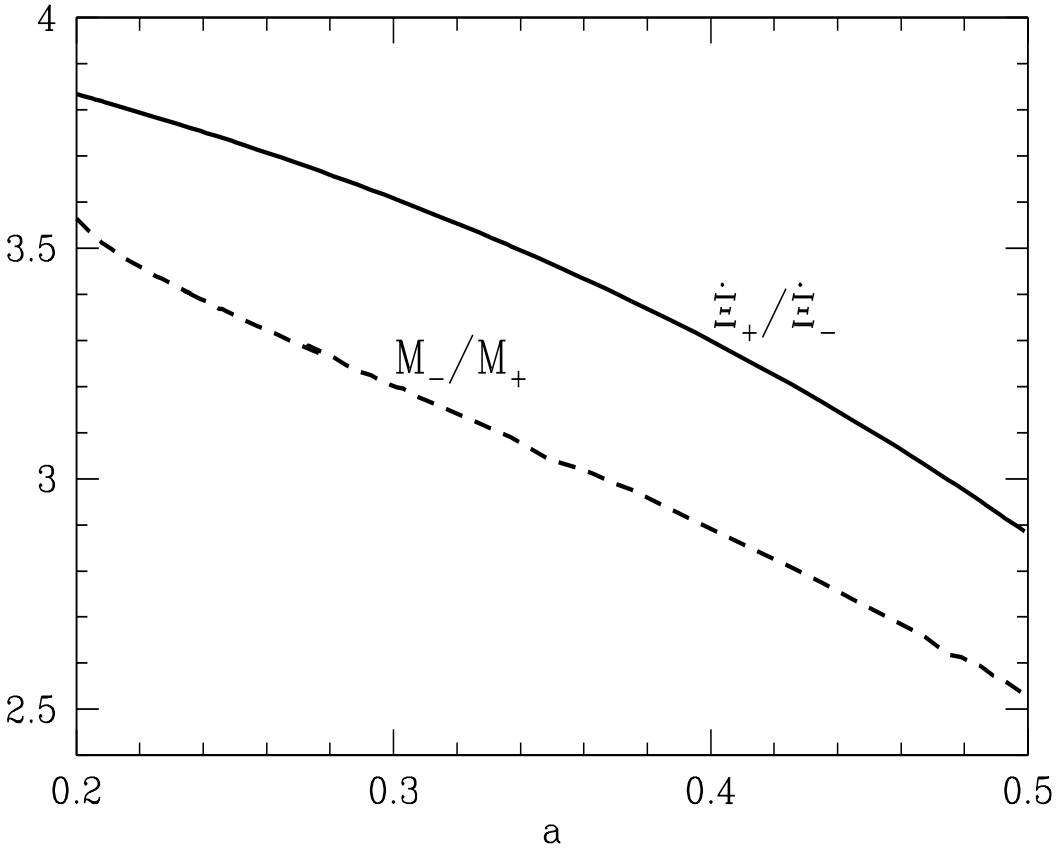

Figure 5b

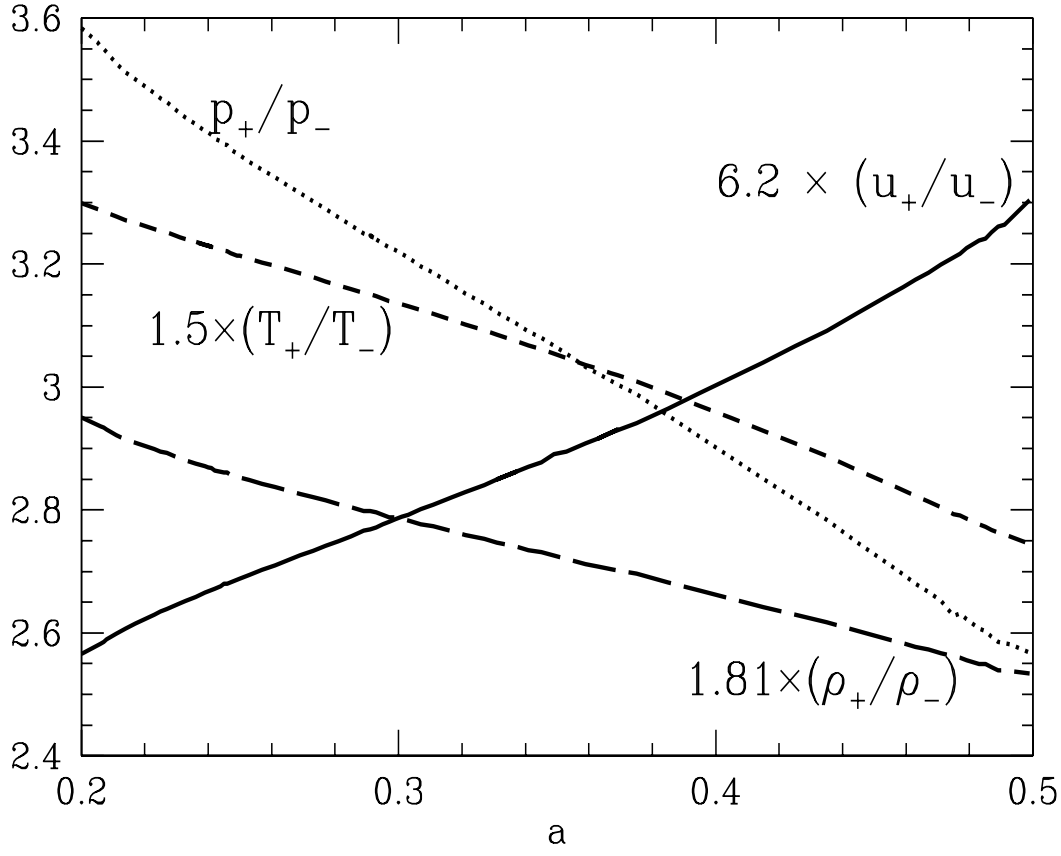

Figure 5c

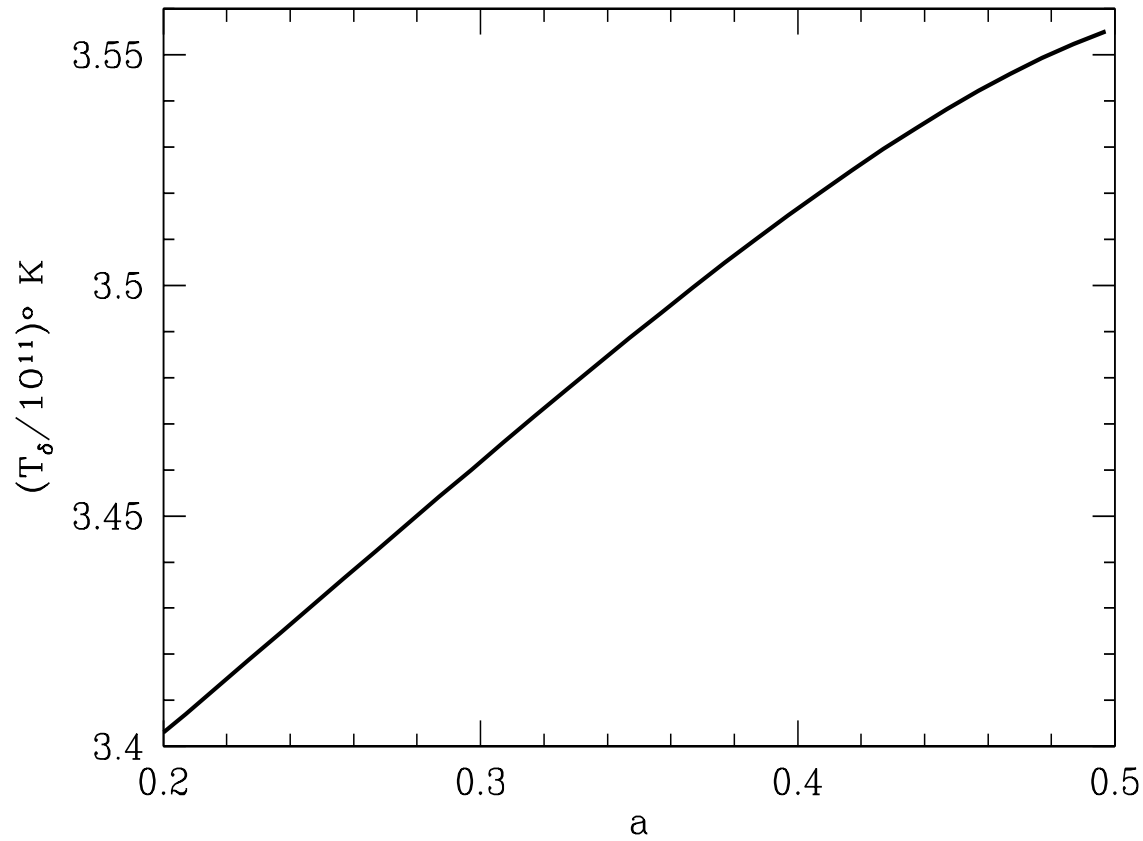

Figure 6a

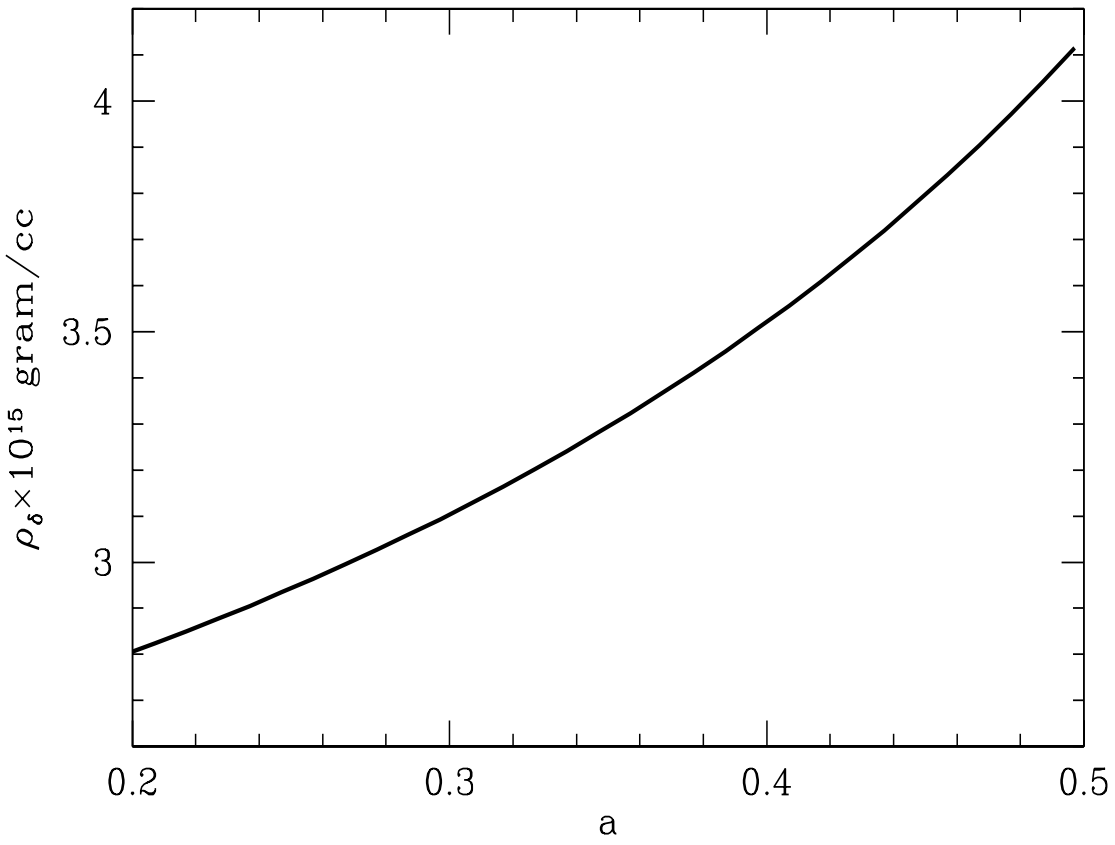

Figure 6b

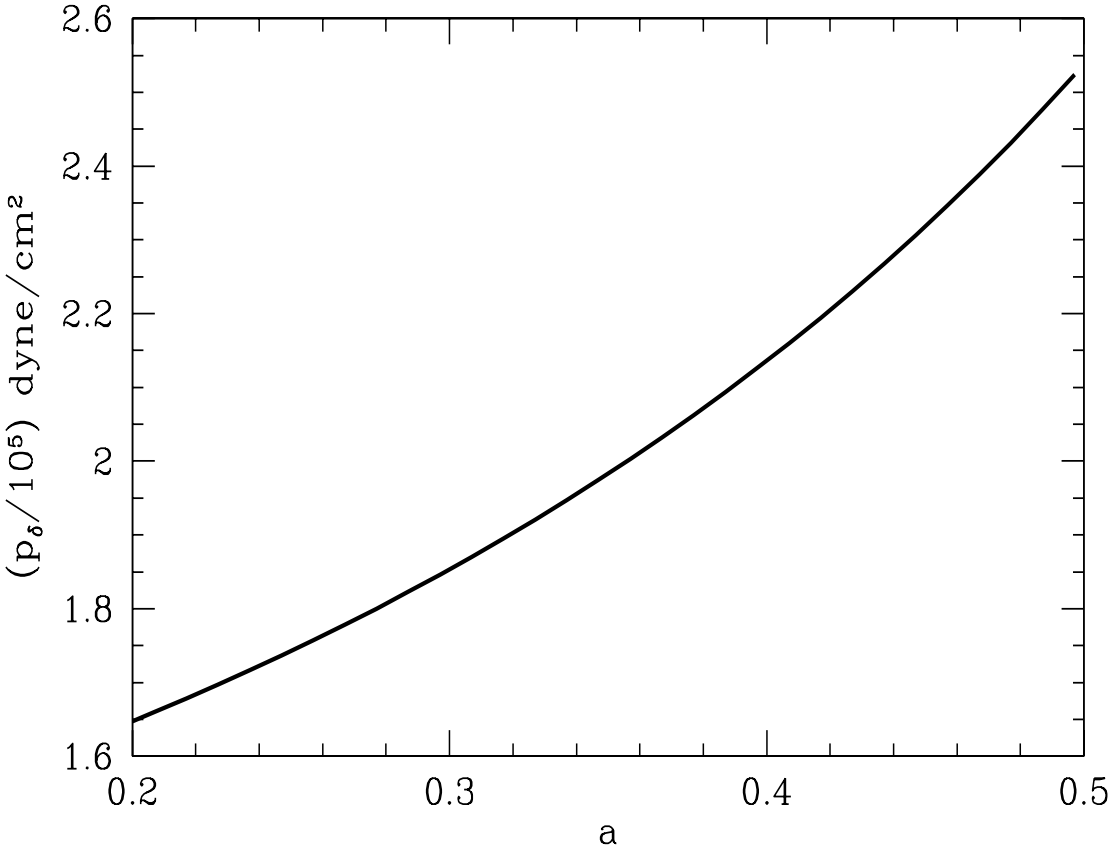

Figure 6c